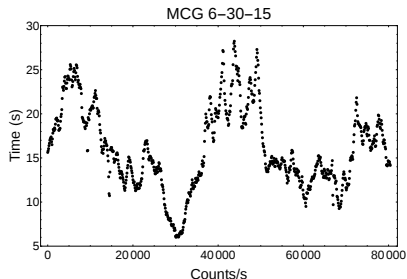# Variability from radiatively driven relativistic jets

P. Mohan[†] & A. Mangalam[‡]

[†]Post Doctoral Fellow,
Aryabhatta Research Institute of Observational Sciences
(ARIES), Nainital, India.

[‡]Associate Professor,
Indian Institute of Astrophysics,
(IIA), Bangalore, India.

Timing studies

MCG 6–30–15

1. Observational: Rapid to long term aperiodic variability: ~ 100 s in γ-rays (e.g. blazars) to months in optical and radio (e.g. blazars, radio galaxies) due to either disk or jet based processes.
2. Theoretical models with diverse explanations: orbital features, disk oscillations, disk viscosity perturbations, shocks in jet, helical motion of blobs in jet and others.

Jet variability models: Mohan & A. Mangalam, 2015, ApJ

- ▶ Bulk flow along funnel shaped magnetic surface with foot-points on the disk (close to the ISCO radius).

- ▶ GR effects considered: Schwarzschild geometry, light bending, aberration, time delay, gravitational and Doppler shifts.

- ▶ Applicable to: jet dominated black hole systems (e.g. Blazars, Quasars, radio galaxies, X-ray binaries, etc.), Neutron stars.

- ▶ Motivations:
  Disk-jet connection in X-ray binaries (e.g. Markoff et al. 2005).
  Emission region could be inside of the ISCO ($5.5 \pm 0.4\ R_s$) from VLBI observations of M87 (Doeleman et al. 2012).
  VLBI knots and optical variability in blazars attributed to rotating jet plasma blobs (Camenzind & Krockenberger 1992; Steffen et al. 1995).
  Pulse profiles of millisecond pulsars produced by X-ray hot-spots in a rapidly rotating neutron star (Poutanen & Beloborodov 2006).

Kinematics of and emission from jets

- ► Radiation driven inner region.
- ► Full general relativistic (GR) model of jet kinematics and blob emission in AGN.
- ► Simulation of LCs from orbiting blob in helical motion along a funnel (or cone) shaped magnetic surface anchored to the accretion disk.
- ► GR effects in Schwarzschild geometry: Doppler and gravitational shifts, aberration, light bending and time delay.
- ► Simulations of kinematics, emission and the power spectral density (PSD) shape and draw conclusions from any trends inferred to compare with observations.
- ► Models applicable to radio, optical and X-ray variability from a wide class of jetted sources: AGN, X-ray binaries, supermassive binary black holes with precessing jets and other compact sources such as neutron stars.

Working Paradigm
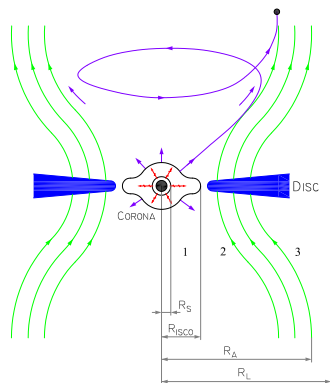
Figure : Kinematically different zones in blob trajectory. Zone 1 ($R_s < r < R_{ISCO}$): radiation pressure dominates outflow kinematics. Zone 2 ($R_{ISCO} < r < R_A$): flow is driven by radiation and co-rotating magnetic field lines anchored to the disk. Zone 3 ($R_A < r < R_L$): inertia dominates, orbital angular momentum of blob has reached an asymptotic value.

Zone 1: outflow kinematics and radiation forces

Four-velocity of blobs:

$$u_\beta = (-(1 - 2M/r)^{1/2}\gamma, (1 - 2M/r)^{-1/2}\beta_r\gamma, r\beta_\theta\gamma, r\sin\theta\beta_\phi\gamma). \quad (1)$$

Four-acceleration of blobs:

$$a^\alpha = \frac{du^\alpha}{d\tau} + \Gamma^\alpha_{\mu\nu}u^\mu u^\nu. \quad (2)$$

Radiation energy flux:

$$F^\alpha = (\delta^\alpha_\mu + u^\alpha u_\mu)T^{\mu\nu}u_\nu, \quad (3)$$

Energy density tensor:

$$T^{(i)(k)} = \int I(r)n^{(i)}n^{(k)}d\Omega \quad (4)$$

where $I(r)$ is the radiation field intensity.

For σ being the cross section of the orbiting blob over which the radiation force acts, Force equation: $\sigma F^\alpha = mc^2 a^\alpha$
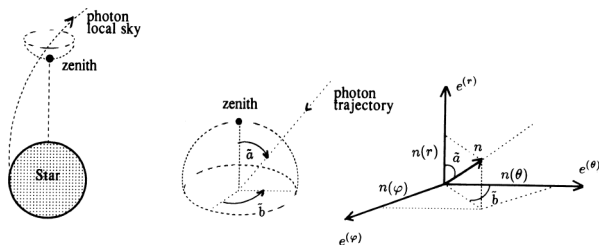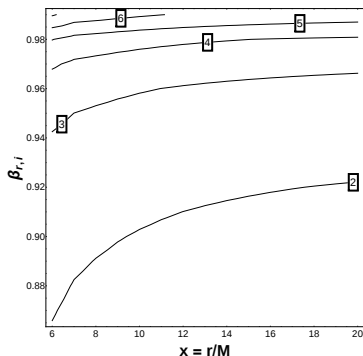
Radiation Geometry

Figure : Local sky of the observer, Fig. courtesy: Abramowicz et al. 1990
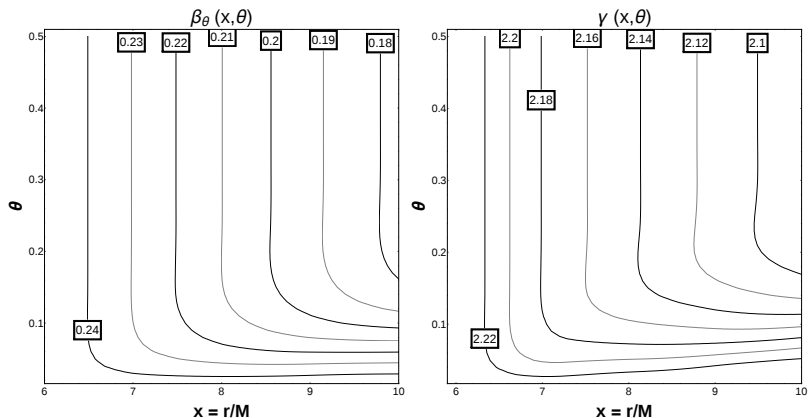
Zone 1: Radial flow ($\beta_\phi = 0$ and $\beta_\theta = 0$) and saturation γ_r

$$\sigma F^r = mc^2 a^r \to (1 - 2/x)\gamma_r^2 \beta_r \frac{d\beta_r}{dx} + \frac{1}{x^2} = \frac{\Gamma_\epsilon}{x^2} \left(\frac{1 - 2/X}{1 - 2/x} \right)^{3/2} \tag{5}$$

$$\left[-\sin^2 \eta (1 + \beta_r^2) + \frac{2}{3}\beta_r(4 - \cos^3 \eta - 3\cos \eta) \right],$$

Zone 1: Poloidal flow ($\beta_\phi = 0$) saturation γ

Figure : Contour plots of $\beta_\theta(x, \theta)$ and $\gamma(x, \theta) = (1 - \beta^2)^{-1/2}$ where $\beta = (\beta_r^2 + \beta_\theta^2)^{1/2}$ for $\beta_{r,i} = 0.86 - 0.99$ and $\beta_{\theta,i} = 0.25 - 0.61$. Left plot: simulated β_θ are in the range $0.18 - 0.81$. The decrease in β_θ is large for smaller initial values of x. Right plot: the decrease in γ also follows the same expected trend to that of β_θ. The simulated γ are in the range $1.1 - 26.3$ higher than in the purely radial case though with saturation of γ to low values occurring even at smaller x. These effects can be attributed to the drag force acting to rapidly cause the loss of any initial angular momentum as well as stabilize the flow at small x.

Zone 3: Illustration of the trajectory of emitting blobs
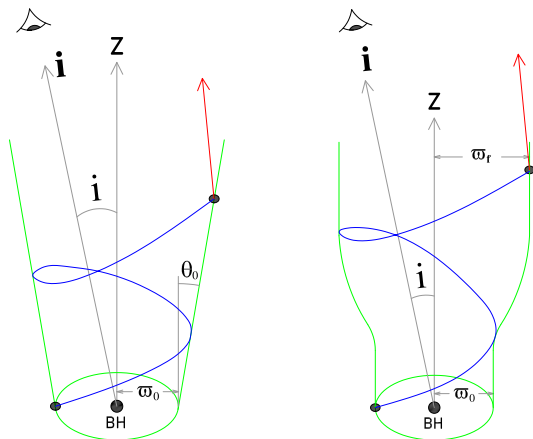
Figure : Helical trajectory of an emitting blob in Schwarzschild geometry, constrained along rotating magnetic field lines with footpoints on a Keplerian disk (at cylindrical radius ϖ_o). In the cone model (left plot), the half opening angle of the jet is θ_0. In the funnel model (right plot), the flow is asympotically bound by a cylinder of radius ϖ_f at large z. The blob trajectory is shown in blue, emission vector in red, geometrical quantities including distances in grey and the jet magnetic surface shape in green.

Figure : If the time of emission is t_{em}, the time at which the signal is observed $t_{obs} = (t_{em} - t_{adv} + \Delta t_{LB})(1 + z)$ where t_{adv} is the time taken for the source to traverse the distance $R \cos \psi$ and Δt_{LB} is the correction due to light bending effect in curved space-time. The blob trajectory is shown in blue, emission vectors in black and geometrical quantities including distances in grey.

Light curve

The effective redshift factor g

$$g = \frac{E_{\text{observed}}}{E_{\text{emitted}}} = \frac{(1 - 2M/R)^{1/2}}{\gamma_{jet}(1 - \beta_{jet} \cos \xi)}. \tag{6}$$

$$\cos \xi = \frac{\dot{\mathbf{x}}_{\mathbf{s}} \cdot \mathbf{k_0}}{|\dot{\mathbf{x}}_{\mathbf{s}}|} = \frac{1}{|\dot{\mathbf{x}}_{\mathbf{s}}|} \left(\frac{\sin \alpha}{\sin \psi} \dot{\mathbf{x}}_{\mathbf{s}} \cdot \mathbf{k} + \frac{\sin(\psi - \alpha)}{\sin \psi} \dot{\mathbf{x}}_{\mathbf{s}} \cdot \mathbf{n} \right). \tag{7}$$

The light curve is given by $F(t_{em}) = g^{2+\Gamma}(t_{em})$ where Γ is the slope in the relation $F_\nu \propto \nu^\Gamma$ between the spectral flux F_ν and the emission frequency in the observer frame.

Fully relativistic funnel model

- Fully relativistic: time delay due to light bending, Doppler and gravitational redshift.
- Kinematics of blobs in funnel model, angular momentum conservation along magnetic surface.
- The cylindrical distance $\varpi(z)$ is given by

$$\varpi(z) = \varpi_0(1 + k(1 - e^{-z/z_f})), \qquad (8)$$

where $k = (\varpi_f - \varpi_0)/\varpi_0$, ϖ_f is the cylindrical distance between the normal axis and the source position at the location where the funnel transitions into a cylinder.

Fully relativistic funnel model
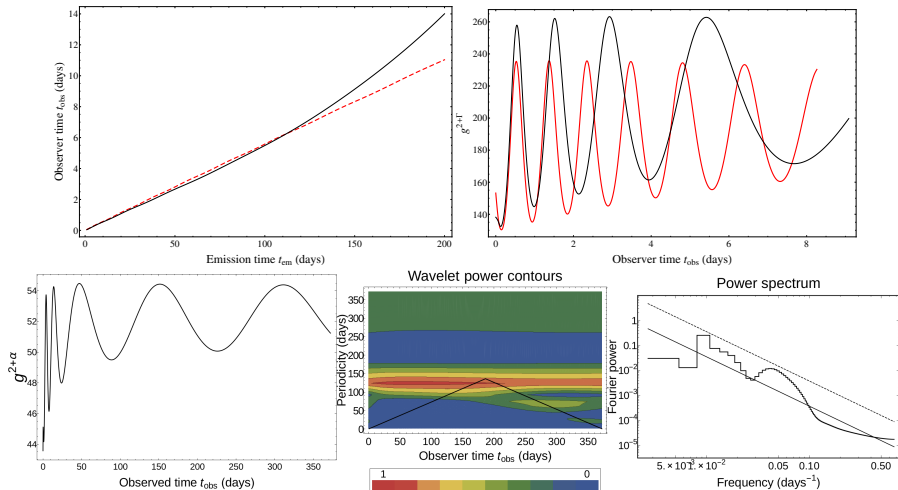
Summary

- Effects of radiation pressure and drag on saturation Lorentz factors $(1.1 - 2.3)$.

- Extension of light-house model proposed in Camenzind & Krockeberger (1992) to full general relativistic.

- g factor: gravitational and Doppler shifts, aberration, time delay due to orientation and light bending.

- Fully relativistic models: amplitude increase (~ 12 %) due to the GR boosts; increasing phase lag between GR and SR light curves.

- Power spectrum slope ~ 2, similar to that observed in Optical and X-ray light curves of blazars.

- QPOs peaked between 1.37 - 130.7 days are inferred from the wavelet and PSD analysis.

- Applicability: BL Lac objects and blazars, binary black holes and X-ray binaries, neutron stars.

Other Applications

Stellar mass Black holes Systems

- ▶ Models of QPOs in the power spectra of accreting, rapidly rotating black holes that originate from the geometric "light echoes" of X-ray flares occurring within the black hole ergosphere. Our plan is to extend previous treatment to three-dimensional photon emission photon orbits in Kerr Geometry.

- ▶ Response functions of a given geometry and use them to produce model light curves we consistently expect QPOs at frequencies on the order of kHz for stellar-mass black hole candidates, while on the order of mHz for typical AGN ($10^7 M_\odot$).

- ▶ The QPO signal is produced by the frame-dragging of the photons by the rapidly rotating black hole, which results in photon "bunches" separated by constant time lags, the result of multiple photon orbits around the hole.

Neutron Star Systems:

- ▶ The Neutron star Interior Composition ExploreR (NICER): an Explorer mission of opportunity for soft x-ray timing spectroscopy.

- ▶ X-ray intensity grow and fall as hot-spots on a neutron star surface spin through the line of sight. The far-side spot becomes more visible for smaller stars through gravitational light-bending, which depends on M/R; thus, depth of modulation constrains compactness.

- ▶ Searches for QPOs and discovery of neutron star rotation rate, is important for eventual light curve analysis, characterization of orbits and component masses in binaries, and for understanding the origins of kHz QPOs, which probe the extreme neutron star environment.

- ▶ Using the fractional amplitudes of the fundamental and the second harmonic of the pulse profile in addition to the amplitude and phase difference of the spectral color oscillations, we can quantify the signal-to-noise ratio necessary to achieve a specified measurement precision for neutron star radius.